Progress In Electromagnetics Research M, Vol. 91, 19–28, 2020

Circularly Polarized Two-Port MIMO Dielectric Resonator Antenna

Gaurav Varshney[1, *], Rakesh Singh[2], Vinay S. Pandey[3], and Rajveer S. Yaduvanshi[4]

Abstract—A two port multi-input-multi-output (MIMO) dielectric resonator (DR) antenna (DRA) is proposed with circularly polarized radiation. The antenna geometry allows to find circular polarization and improved impedance bandwidth by reducing the separation between the DR elements. The isolation between the ports of the antenna remains more than 15 dB in the operating passband even after reducing the separation between the radiating elements. The antenna provides the 10-dB impedance and 3-dB axial ratio bandwidth of 34.85% and 4.55%, respectively. The MIMO performance of the proposed antenna is confirmed by calculating the parameters like envelop correlation coefficient, diversity gain, mean effective gain, channel capacity loss, and the total active reflection coefficient. The proposed antenna can be utilized for C-band applications.

1. INTRODUCTION

The dielectric resonator antenna (DRA) has the features like high gain and radiation efficiency, wide bandwidth, and low losses which make it prominent over conducting surface antennas [1]. Nowadays, the advancement in communication system needs higher data transfer rate which can be obtained by using multi-input multi-output (MIMO) technology. In this motif, some MIMO DRAs have been implemented and reported in the literature [2–7]. In the design of a MIMO antenna system, the main requirement remains to obtain the high isolation between the ports and the lowest envelope correlation coefficient (ECC). In order to fulfill these requirements, MIMO antennas have been developed with the multi-radiators having an appropriate spacing between them [8–11]. The spacing between the radiators reduces the mutual coupling and hence the isolation. However, the MIMO antennas with multi-radiators have the major limitation of larger antenna size. To prevent this limitation, MIMO antennas have been implemented with a single radiator, and feeding is applied such that the orthogonal modes could be generated [6, 12–14]. The generation of orthogonal modes reduces ECC of MIMO antenna having single radiator.

Most of the studies on MIMO DRAs, which have been carried out till now, are reported with linearly polarized (LP) radiations [8–10, 15]. The limitation of LP antennas is the polarization mismatch losses. This can be prevented by the generation of circular polarization in the antenna [16, 17]. In the literature, very few MIMO DRAs have been reported with circularly polarized (CP) response [11, 18, 19]. The antenna geometry presented in [11] utilizes the cylindrical DRs excited using tilted aperture slots. In [19], two separated L-shaped DR elements have been utilized with a defected ground structure for obtaining the CP response in a two-port MIMO antenna. The limitation of these antenna structures is large antenna size due to widely separated radiating elements. A two-port cross-shaped DR has also been reported with single radiator in [18], but it utilizes a complex feeding mechanism and provides CP radiation with single port only. At another port, it provides linearly polarized radiation. Thus, in the current scenario, the main research issues are (i) obtaining the CP radiations in the MIMO antenna,

Received 10 January 2020, Accepted 27 March 2020, Scheduled 1 April 2020
* Corresponding author: Gaurav Varshney (gauravnitd@outlook.com).
[1] ECE Department, National Institute of Technology Patna, 800005, India. [2] ECE Department, IIT Roorkee, 110040, India.
[3] Applied Sciences, NIT Delhi, 110040, India. [4] ECE Department, AIACTR Delhi, 110031, India.

(ii) reduction in the separation between the radiating elements, and (iii) maintaining the high isolation between the ports. In this motif, a technique has been implemented using which the solution of all the above problems can be found. A two-port MIMO DRA is reported with the CP response. The antenna geometry is selected and arranged in such a manner that placing the DRs with zero separation aligns the field vectors orthogonally as the hybrid of modes $TM_{11\delta}$ and $TM_{21\delta}$, which provides the CP radiation [20]. The antenna provides the CP response with the excitation at each port separately. In the literature, the CP radiation has been achieved using the multi-feed network in DRA [21, 22]. The disadvantage of the multi-feed network is that it requires an external power divider and makes the antenna structure bulky [23]. The proposed antenna provides the advantage over the antenna structures with multi-feed mechanism by preventing the use of external power dividers.

In the proposed antenna, placing the DRs without separation, increases the length to width aspect ratio which enhances the impedance bandwidth. The proposed antenna provides a wideband response with the measured impedance bandwidth of 36.71% at each port. The antenna structure offers the isolation between the ports more than 15 dB after placing DRs with no separation between them. The MIMO performance parameters like ECC, diversity gain (DG), mean effective gain (MEG), channel capacity loss (CCL), and total active reflection coefficient (TARC) remain in the acceptable limits. Thus, the proposed technique offers the advantage of CP radiations and zero separation between the DR elements of the MIMO antenna over the other existing antennas reported in [9–11, 15, 19].

2. ANTENNA DESIGN AND ANALYSIS

Figure 1(a) shows the geometry of the proposed two-port MIMO DRA. The antenna structure consists of a substrate of FR-4 epoxy having permittivity $\epsilon_s = 4.4$ and dimensions $l_s \times w_s$ at the top of the ground plane. A combination of a rectangular DR having dimensions $a \times b \times h$ and half-cylinder having radius r is placed above the substrate. The dimensions of the half-cylindrical DR are selected for the resonant frequency of the operating fundamental mode $TM_{11\delta}$ using the formulae and analysis given in [20, 24]. After calculation, the dimensions of the antenna are optimized using full wave simulator to find the desired results. The material TMM13i having relative permittivity, $\epsilon_r = 12.8$, is used in dielectric resonator. The electrical and physical properties of the TMM13i remain approximately constant over a wide range of temperature variation [25]. It is assumed that the characteristics of the antenna will be approximately same within the operating frequency range with the variation of temperature between 0° and 140° [25]. The RF excitation is applied using 50Ω microstrip lines of dimensions $l_m \times w_m$ and conformal patch of height h_p at the edges of the DR as shown in Fig. 1(b). Similar and opposite DR arrangements are placed without separation between them. The antenna structure is designed and analyzed using high frequency structure simulator and fabricated. Fig. 1(c) shows the fabricated prototype of the proposed antenna. Moreover, the proposed antenna dimensions are selected for operating in the C-band of microwave frequency. The antenna dimensions can also

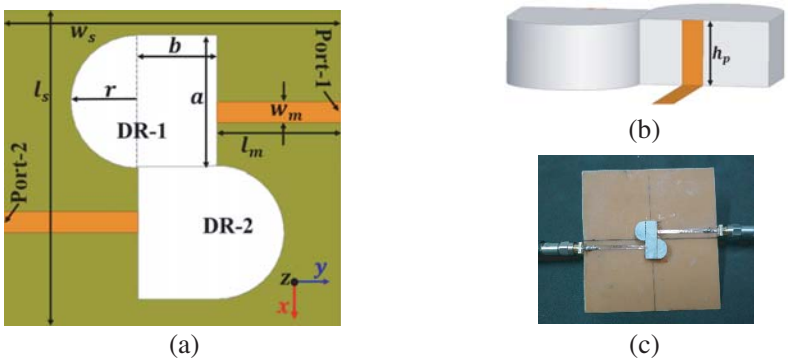

Figure 1. (a) The antenna geometry, (b) side view of the DR and (c) fabricated antenna prototype. $l_s = 80$, $w_s = 80$, $l_m = 37$, $w_m = 1.6$, $a = 10.1$, $b = 6$, $r = 5.2$, $h = 5$ and $h_p = 5$ (the unit of the dimensions is mm).

be scaled to operate with the applications of different frequency bands while the structure can be set similar for obtaining a similar kind of antenna response.

3. RESULTS AND DISCUSSION

To understand advantages of the proposed technique, two antenna structures are designed as shown in Fig. 2. In antenna-1, the DR elements are separated with the distance equivalent to half-wavelength. In antenna-2, the DR elements are placed without any separation between them. Fig. 3 shows the comparison of S-parameter responses of these antennas, and their performance is reported in Table 1. It can be observed in Fig. 3(a) that the impedance matching of the antenna is improved in the case of antenna-2, and a wide 10-dB impedance bandwidth is achieved. Each single DR element of antenna-1 operates with $TM_{11\delta}$ and $TM_{21\delta}$ modes at frequencies 6.44 and 7.88 GHz, respectively. Fig. 4 shows E- and H-field distributions in the single DR element of antenna-1, which confirms the generation of these modes. The geometry of the single DR element is quite close to the elliptical shape. Earlier, TM modes have been excited in such a geometry [26, 27]. Also, the field distributions of these modes excited in the proposed DR geometry are quite similar to the field distribution reported in a half cylindrical DR [20]. Moreover, the excitation of these modes provides radiations in the boresight direction correlating with the investigations reported in a half-cylindrical [20, 28] and half-hemispherical DRA [29]. Antenna-1 provides high-reflected power at the frequency of fundamental hybrid mode. Placing the DR elements without separation increases the length to width aspect ratio because they start operating as a single DR, and hence the antenna provides good impedance matching at the frequency of fundamental mode which results in a wider impedance bandwidth [30].

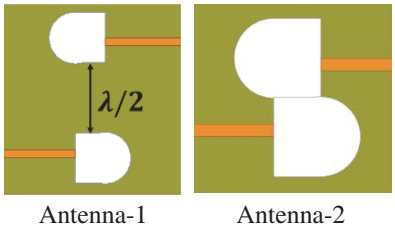

Figure 2. Two antenna structures.

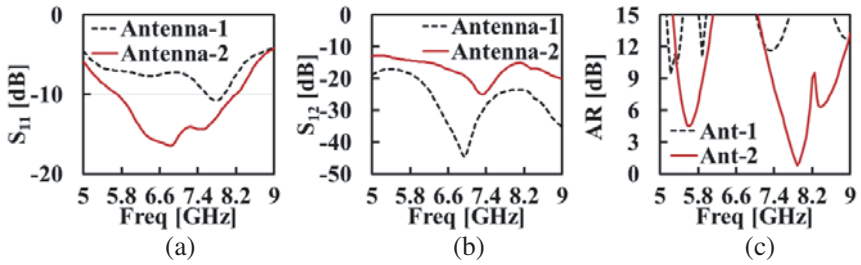

Figure 3. The frequency response of antenna-1 and 2 (a) S_{11}-parameter, (b) S_{12}-parameter and (c) AR.

Table 1. Performance of antenna-1 and 2.

Antenna	Spacing between DR elements	10-dB Impedance bandwidth (%)	Isolation (dB)	3-dB AR bandwidth (%)
1	$\lambda/2$	4.89 (7.57–7.95 GHz)	20	0
2		35.80 (5.71–8.2 GHz)	15	4.06 (7.72–8.04 GHz)

Figure 3(b) shows the plot for isolation between the ports in antenna-1 and 2. The isolation is reduced in the case of antenna-2 when the DR elements are kept closer to each other. However, the minimum isolation between the ports of the antenna remains 15 dB in the operating passband, which can be accepted for the operation of the MIMO antenna [14]. The reason of reduction in the isolation is the reduction in the distance between DR elements [8]. However, the reduction in the separation between the DR elements generates the orthogonal field components which results in the CP response. Fig. 3(c) shows the axial ratio (AR) of both the antennas. In the case of antenna-2, placing the DR elements without separation generates orthogonal modes. This brings the AR below 3-dB providing the CP response at frequency 7.88 GHz. Fig. 5(a) shows the field distribution at frequency 6.44 GHz in the proposed two-port MIMO antenna. In both, lower and upper partd of the DR, the field distribution is

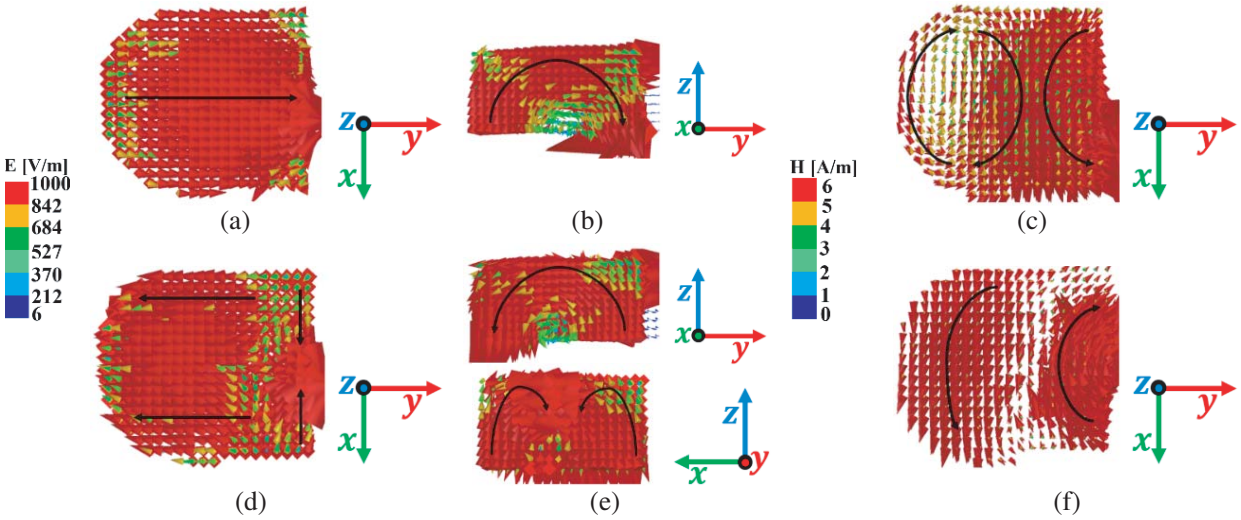

Figure 4. (a), (b) E and (c) H-field distribution at frequency 6.44 GHz ($TM_{11\delta}$ mode). (d), (e) E and (f) H-field distribution at frequency 7.88 GHz ($TM_{21\delta}$ mode).

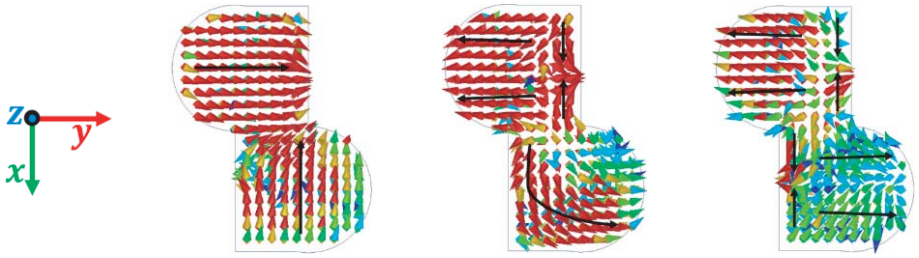

Figure 5. E-Field distribution in the combined DR elements at frequency (a) 6.44 (b) 7.72 and (c) 8.02 GHz.

corresponding to mode $TM_{11\delta}$. At this frequency, the antenna provides LP radiation. Figs. 5(b) and (c) show the field distributions at frequency 7.72 and 8.02 GHz, respectively. At frequency 7.72 GHz, the field is similar as $TM_{21\delta}$ mode in the upper part and as $TM_{11\delta}$ mode in the lower part of the DR. At frequency 8.02 GHz, the field is distributed as $TM_{21\delta}$ mode in both parts of DR. Thus, it can be noted that the field distribution in the upper part of the DR remains same as $TM_{21\delta}$ mode at both the operating frequencies while it is changed from $TM_{11\delta}$ to $TM_{21\delta}$ with the change in the operating frequency from 7.72 to 8.04 GHz. The frequencies 7.72 and 8.02 GHz are at around $+45°$ and $-45°$ points from the center frequency 7.88 GHz at which CP is achieved. Thus, it can be concluded that there is a phase difference of 90° between $TM_{11\delta}$ and $TM_{21\delta}$ modes generated in the lower part of the DR. It is already reported that the excitation of these modes with the phase difference of 90° between them provides the CP fields [20, 24]. Observing the field distribution at frequency 7.88 GHz shown in Fig. 6(a), it can be observed that it is a hybrid of modes $TM_{21\delta}$ and $TM_{11\delta}$.

For the confirmation of the CP operation, E-field is analyzed at the top surface of the DR at different time instants as shown in Fig. 6. It can be observed that the field vectors rotate at an angle of 90° in a constant — $z = d$ plane after each quarter cycle of the time period T [31]. The CP response and zero separation between the DR elements is obtained at the cost of the reduction in the isolation. However, it remains more than 15 dB in the operating passband.

Figure 7 shows the simulated and measured S-parameter responses of the proposed antenna (antenna-2). The antenna provides the simulated and measured impedance bandwidths of 35.80% (5.71–8.2 GHz) and 36.71% (5.67–8.22 GHz), respectively at both the ports. The symmetricity of the

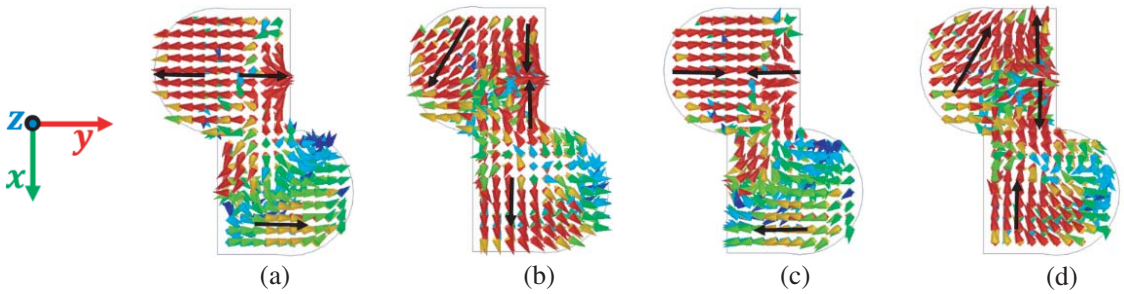

Figure 6. The E-field distribution at frequency 7.88 GHz at time t = (a), (b) $T/4$, (c) $T/2$ and (d) $3T/4$.

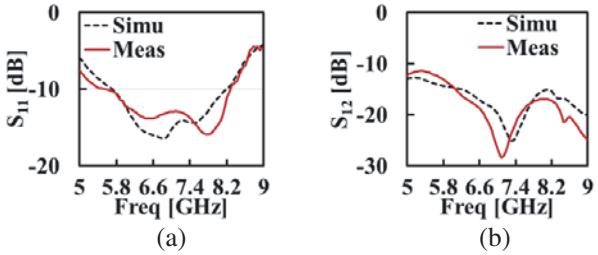

Figure 7. Simulated and measured frequency response of (a) S_{11} and (b) S_{12}-parameter.

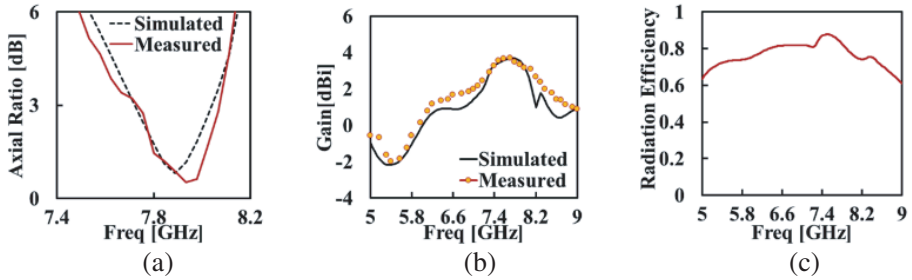

Figure 8. Simulated and measured (a) AR, (b) gain and (c) simulated radiation efficiency.

antenna structure provides $S_{11} = S_{22}$. The simulated and measured values of isolation remain 15 dB or more in the passband. The far-field properties of the antenna like radiation pattern, AR, and gain are measured using the satimo start lab system. Fig. 8(a) shows the simulated and measured ARs in the boresight direction ($\theta = 0°$). The antenna provides the simulated and measured 3-dB AR bandwidths of 4.06% (7.72–8.04 GHz) and 4.55% (7.72–8.08 GHz), respectively. The antenna provides CP radiation with the excitation at both the ports. Fig. 8(b) shows the gain plot of the antenna in the boresight direction. The antenna provides the peak of gain around 3.8 dBic in the passband where CP is achieved. Fig. 8(c) shows the simulated radiation efficiency, which remains around 80% in the passband. Figs. 9 and 10 shows the radiation patterns with the excitation at both the ports at frequencies 6.44 and 7.93 GHz, respectively. The antenna provides the LP radiations at frequency 6.44 GHz and CP radiation at frequency 7.93 GHz. The separation between co- and cross-polarized components remains 18 dB or more in the boresight direction ($\theta = 0°$) in both the principal planes. The antenna provides the radiation with dominant (co-polarized) right-hand CP field at frequency 7.93 GHz.

4. MIMO AND DIVERSITY PERFORMANCE

The MIMO performance of antenna is verified by calculating parameters ECC, DG, MEG, CCL, and TARC. Fig. 11 shows the plots for these parameters. The ECC is calculated using measured

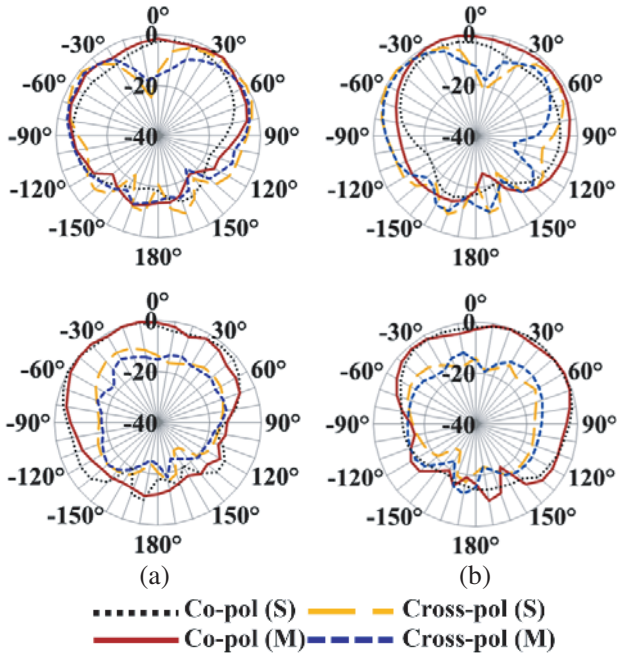

Figure 9. Radiation pattern of the antenna at frequency 6.44 GHz at (a) port-1 and (b) port-2 (upper images in xz-plane and lower images in yz-plane).

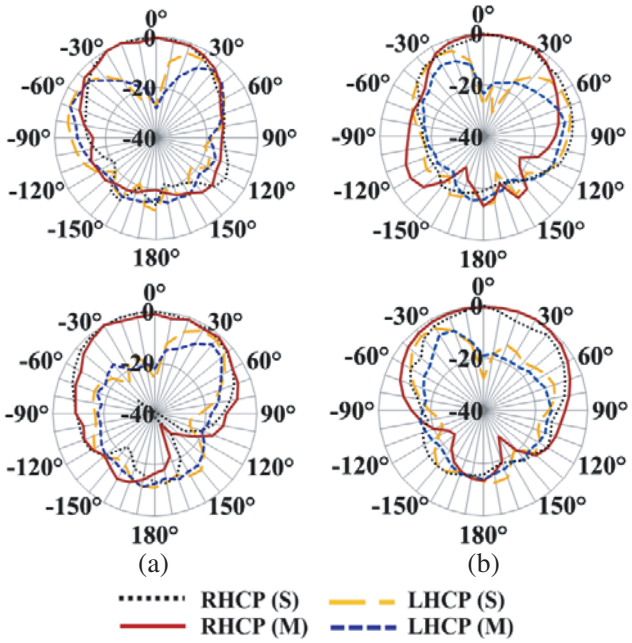

Figure 10. Radiation pattern of the antenna at frequency 7.93 GHz at (a) port-1 and (b) port-2 (upper images in xz-plane and lower images in yz-plane).

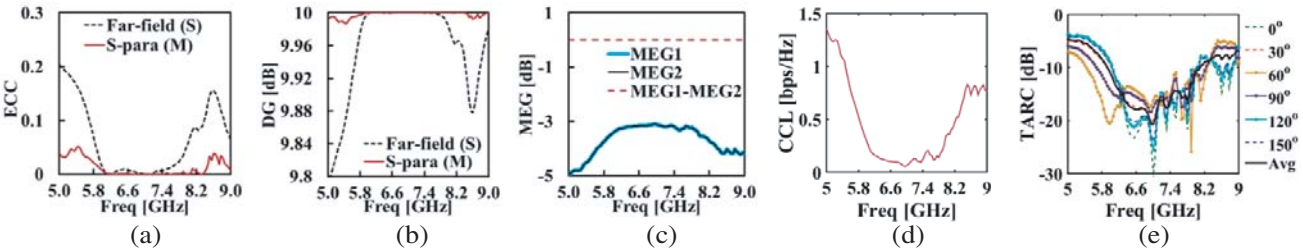

Figure 11. (a) ECC, (b) DG, (c) MEG, (d) CCL and (e) TARC (for seven values of input phase angle (θ)) (S-simulated, M-measured).

S-parameters and simulated far-field parameters using Eqs. (1) and (2) [10, 32].

$$\rho_{eij} = \frac{\left|S_{11}^{*}S_{12} + S_{21}^{*}S_{22}\right|^{2}}{\left(1-\left(|S_{11}|^{2}+|S_{21}|^{2}\right)\right)\left(1-\left(|S_{22}|^{2}+|S_{12}|^{2}\right)\right)} \tag{1}$$

$$\rho_{eij} = \left|\frac{\iint (E_{\theta i}.E_{\theta j}^{*} + E_{\phi i}.E_{\phi j}^{*})d\Omega}{\iint (E_{\theta i}E_{\theta i}^{*} + E_{\phi i}.E_{\phi i}^{*})d\Omega \iint (E_{\theta j}E_{\theta j}^{*} + E_{\phi j}.E_{\phi j}^{*})d\Omega}\right|^{2} \tag{2}$$

Here, ρ_{eij} is ECC of the i^{th} and j^{th} antenna elements, and Ω is the solid angle. The acceptable value of ECC is less than 0.5 [33]. For the proposed antenna, the ECC remains less than 0.05 in the passband as shown in Fig. 11(a).

The DG of the antenna is calculated using mathematical evaluation reported in [4]. The DG of the antenna should be greater than 9.95 in the operating passband. Fig. 11(b) shows the simulated and measured plot for DG. It remains around 10 dB in the passbands, which shows that the antenna

provides a good MIMO performance.

$$G_d = 10e_p \quad \text{where} \quad e_p = \sqrt{\left(1 - |0.99\rho_e|^2\right)} \tag{3}$$

The MEG is calculated at both ports using [34]. It remains around 3 dB. The difference between MEGs at port-1 (MEG_1) and at port-2 (MEG_2) is near 0 dB as shown in Fig. 11(c).

$$MEG_i = 0.5\eta_{i,\,rad} = 0.5\left[1 - \sum_{j=1}^{M} |S_{ij}|^2\right] \tag{4}$$

where M is the number of ports in MIMO antenna, and $\eta_{i,\,rad}$ is the radiation efficiency of the antenna. Fig. 11(d) shows CCL of the proposed antenna. It is calculated using the method reported in [35]. The CCL of the proposed antenna remains below the acceptable range (CCL < 0.5 bps/Hz) in the operating passbands.

$$CCL = -\log_2 \det(\psi^R) \tag{5}$$

$$\psi^R = \begin{pmatrix} \rho_{e11} & \rho_{e12} \\ \rho_{e21} & \rho_{e22} \end{pmatrix} \tag{6}$$

TARC is the ratio of square root of total reflected power to the square root of total incident power. It is calculated using Eq. (8). Fig. 11(e) shows the calculated TARC of the antenna for seven different values of the input phase angles [36, 37]. The reflection coefficient of the antenna is quite stable for different values of the input phase angle.

$$\Gamma_a^t = \frac{\sqrt{\sum_j^M |b_j|^2}}{\sqrt{\sum_j^M |a_j|^2}} \tag{7}$$

Where a_j is the incident wave, and b_j is reflected wave. The dependency of TARC on S-parameters is defined as [36].

$$\Gamma_a^t = \sqrt{\frac{|S_{11} + S_{12}e^{j\theta}|^2 + |S_{21} + S_{22}e^{j\theta}|^2}{2}} \tag{8}$$

Table 2. Comparison of the proposed antenna with other two-port MIMO DRA.

Ref	DR Shape	Number of DR Elements	Spacing between the DR elements	f_r (GHz)	f_{CP} (GHz)	BW_{AR} (%)	BW_{Im} (%)		Isolation (dB)	Gain (dBi)	
							P_1	P_2		P_1	P_2
[8]	F	Two	$\lambda/3$	2.5	–	0	36	31	27	1.99	1.85
[9]	A	Two	$\lambda/4$	3.65	–	0	59.2	60.9	20	–	
[10]	Mushroom	Two	$\lambda/4$	5.37	–	0	61	65	20	–	
[15]	Tree	Two	$\lambda/4$	5.6	–	0	89.9		17	–	
[11]	Cylindrical	Two	$\lambda/4$	5.75	5.75	3.50	15.1	14.9	23	4.7	
[19]	L	Two	$\lambda/3$	5.5	5.4	4.60	17.16		15	3.8	
This Antenna	**Rectangular and half-cylinder**	**Two**	**0**	**6.44**	**7.88**	**4.55**	**36.71**		**15**	**3.8**	

f_r −resonant frequency of fundamental mode, f_{CP} −centre frequency at which CP is achieved, BW_{AR} −3-dB AR bandwidth, BW_{Im} −10-dB impedance bandwidth, P_1 −port-1 and P_2 −port-2 (in the case of CP antenna the unit of gain is dBic).

where θ is the phase of the input signal.

Table 2 shows the comparison of the proposed antenna with the other MIMO DRAs. It can be observed that the proposed antenna offers the advantage of CP radiations in comparison to the antennas reported in [8–10]. Furthermore, the arrangements of the DR allow to reduce the spacing between the DR elements and provides the CP radiation. This proves that the proposed antenna is a good candidate over other MIMO CPDRAs which are implemented with at least $\lambda/4$ spacing between the DR elements reported in [11, 19]. Also, the isolation and gain of the antenna are comparable with other antennas.

5. CONCLUSION

A two-port multi-input-multi-output (MIMO) dielectric resonator (DR) antenna (DRA) has been implemented with circularly polarized radiation. The reduction in the separation between the DR elements provides the CP radiation and enhanced impedance bandwidth. The isolation of 15 dB or more has been achieved between the ports of the antenna. The antenna provides 10-dB impedance and 3-dB axial ratio bandwidth of 34.85% and 4.55%, respectively. The MIMO performance parameters like envelop correlation coefficient, diversity gain, mean effective gain, channel capacity loss, and the total active reflection coefficient remain in the acceptable limits. The proposed antenna is suitable for C-band applications.

ACKNOWLEDGMENT

Authors are thankful to Mr. Vipin Pasricha, Krishan Kant, A. P. Singh and G. Ravi Kumar, BEL India for their support in the measurement of the results of antenna prototype.

REFERENCES

1. Antar, Y. M. M. and Z. Fan, "Theoretical investigation of aperture-coupled rectangular dielectric resonator antenna," *IEE Proc. — Microwaves, Antennas Propag.*, Vol. 143, No. 2, 113, 1996.
2. Ishimiya, K., Z. Ying, and J. Takada, "A compact MIMO DRA for 802. 11n application," *Antennas and Propagation Society International Symposium*, 4–7, San Diego, CA, USA, 2008.
3. Yan, J. B. and J. T. Bernhard, "Implementation of a frequency-agile MIMO dielectric resonator antenna," *IEEE Trans. Antennas Propag.*, Vol. 61, No. 7, 3434–3441, 2013.
4. Roslan, S. F., M. R. Kamarudin, M. Khalily, and M. H. Jamaluddin, "An MIMO rectangular dielectric resonator antenna for 4G applications," *IEEE Antennas Wirel. Propag. Lett.*, Vol. 13, 321–324, 2014.
5. Das, G., A. Sharma, and R. K. Gangwar, "Wideband self-complementary hybrid ring dielectric resonator antenna for MIMO applications," *IET Microwaves, Antennas Propag.*, Vol. 12, No. 1, 5–11, 2017.
6. Yan, J. B. and J. T. Bernhard, "Design of a MIMO dielectric resonator antenna for LTE femtocell base stations," *IEEE Trans. Antennas Propag.*, Vol. 60, No. 2, 438–444, 2012.
7. Khan, A. A., R. Khan, S. Aqeel, J. Nasir, J. Saleem, and Owais, "Design of a dual-band MIMO dielectric resonator antenna with high port isolation for WiMAX and WLAN applications," *Int. J. RF Microw. Comput. Eng.*, 1–11, 2017.
8. Roslan, S. F., M. R. Kamarudin, M. Khalily, and M. H. Jamaluddin, "An MIMO F-shaped dielectric resonator antenna for 4G applications," *Microw. Opt. Technol. Lett.*, Vol. 57, No. 12, 2931–2936, 2015.
9. Sharma, A., A. Sarkar, A. Biswas, and M. J. Akhtar, "A-shaped wideband dielectric resonator antenna for wireless communication systems and its MIMO implementation," *Int. J. RF Microw. Comput. Eng.*, Vol. 28, No. 8, e21402, 2018.
10. Sharma, A. and A. Biswas, "Wideband multiple-input–multiple-output dielectric resonator antenna," *IET Microwaves, Antennas Propag.*, Vol. 11, No. 4, 496–502, 2017.

11. Das, G., A. Sharma, and R. K. Gangwar, "Dielectric resonator based circularly polarized MIMO antenna with polarization diversity," *Microw. Opt. Technol. Lett.*, Vol. 60, No. 3, 685–693, 2018.
12. Khan, A. A., M. H. Jamaluddin, S. Aqeel, J. Nasir, J. U. R. Kazim, and O. Owais, "Dual-band MIMO dielectric resonator antenna for WiMAX/WLAN applications," *IET Microwaves Antennas Propag.*, Vol. 11, No. 1, 113–120, 2017.
13. Abdalrazik, A., A. S. A. El-hameed, and A. B. Abdel-rahman, "A three-port MIMO dielectric resonator antenna using decoupled modes," *IEEE Antenna Propag. Lett.*, Vol. 16, 3104–3107, 2017.
14. Varshney, G., S. Gotra, S. Chaturvedi, V. S. Pandey, and R. S. Yaduvanshi, "Compact four-port MIMO dielectric resonator antenna with pattern diversity," *IET Microwaves Antennas Propag.*, 1–7, 2019.
15. Trivedi, K. and D. Pujara, "Mutual coupling reduction in wideband tree shaped fractal dielectric resonator antenna array using defected ground structure for MIMO applications," *Microw. Opt. Technol. Lett.*, Vol. 59, No. 11, 2735–2742, 2017.
16. Varshney, G., V. S. Pandey, and R. S. Yaduvanshi, "Axial ratio bandwidth enhancement of a circularly polarized rectangular dielectric resonator antenna," *Int. J. Microw. Wirel. Technol.*, Vol. 10, No. 8, 984–990, 2018.
17. Varshney, G., V. S. Pandey, and R. S. Yaduvanshi, "Dual-band fan-blade-shaped circularly polarised dielectric resonator antenna," *IET Microwaves, Antennas Propag.*, Vol. 11, No. 13, 1868–1871, 2017.
18. Zou, L. and C. Fumeaux, "A cross-shaped dielectric resonator antenna for multifunction and polarization diversity applications," *IEEE Antennas Wirel. Propag. Lett.*, Vol. 10, 742–745, 2011.
19. Kumar, N., S. Gourab, D. Ravi, and K. Gangwar, "L-shaped dielectric resonator based circularly polarized multi-input-multi-output (MIMO) antenna for wireless local area network (WLAN) applications," *Int. J. RF Microw. Comput. Eng.*, 1–11, May 2018.
20. Tam, M. T. K. and R. D. Murch, "Circularly polarized circular sector dielectric resonator antenna," *IEEE Trans. Antennas Propag.*, Vol. 48, No. 1, 126–128, Jan. 2000.
21. Pan, Y., K. W. Leung, and E. H. Lim, "Compact wideband circularly polarised rectangular dielectric resonator antenna with dual underlaid hybrid couplers," *Microw. Opt. Technol. Lett.*, Vol. 52, No. 12, 2789–2791, Dec. 2010.
22. Li, B., C. X. Hao, and X. Q. Sheng, "A dual-mode quadrature-fed wideband circularly polarized dielectric resonator antenna," *IEEE Antennas Wirel. Propag. Lett.*, Vol. 8, 1036–1038, 2009.
23. Varshney, G., V. S. Pandey, R. S. Yaduvanshi, and L. Kumar, "Wide band circularly polarized dielectric resonator antenna with stair-shaped slot excitation," *IEEE Trans. Antennas Propag.*, Vol. 65, No. 3, 1380–1383, 2017.
24. Tam, M. T. K. and R. D. Murch, "Compact circular sector and annular sector dielectric resonator antennas," *IEEE Trans. Antennas Propag.*, Vol. 47, No. 5, 837–842, 1999.
25. Rogers Corporation, "TMM thermoset microwave materials," 2015.
26. Okaya, A. and L. F. Barash, "The dielectric microwave resonator," *Proc. IRE*, Vol. 50, No. 10, 2081–2092, 1962.
27. Tadjalli, A., A. R. Sebak, and T. A. Denidni, "Resonance frequencies and far field patterns of elliptical dielectric resonator antenna: Analytical approach," *Prog. Electromagn. Res.*, Vol. 64, 81–98, 2006.
28. Chaudhary, R. K., K. V. Srivastava, and A. Biswas, "Wideband multilayer multi-permittivity half-split cylindrical dielectric resonator antenna," *Microw. Opt. Technol. Lett.*, Vol. 54, No. 11, 997–999, 2012.
29. Kakade, A. B. and B. Ghosh, "Mode excitation in the coaxial probe coupled three-layer hemispherical dielectric resonator antenna," *IEEE Trans. Antennas Propag.*, Vol. 59, No. 12, 4463–4469, 2011.
30. Chang, T. and J. Kiang, "Bandwidth broadening of dielectric resonator antenna by merging adjacent bands," *IEEE Trans. Antennas Propag.*, Vol. 57, No. 10, 3316–3320, Oct. 2009.

31. Gotra, S., G. Varshney, R. S. Yaduvanshi, and V. S. Pandey, "Dual-band circular polarisation generation technique with the miniaturisation of a rectangular dielectric resonator antenna," *IET Microwaves, Antennas Propag.*, 2019 (Accepted).
32. Blanch, S., J. Romeu, and I. Corbella, "Exact representation of antenna system diversity performance from input parameter description," *Electron. Lett.*, Vol. 39, No. 9, 705, 2003.
33. Sharawi, M. S., "Current misuses and future prospects for printed multiple-input, multiple-output antenna systems," *IEEE Antenna Propag. Mag.*, Vol. 59, No. 2, 162–170, 2017.
34. Nasir, J., M. H. Jamaluddin, M. Khalily, M. R. Kamarudin, I. Ullah, and R. Selvaraju, "A reduced size dual port MIMO DRA with high isolation for 4G applications," *Int. J. RF Microw. Comput. Eng.*, Vol. 25, No. 6, 495–501, 2015.
35. Gotra, S., G. Varshney, V. S. Pandey, and R. S. Yaduvanshi, "Super-wideband multi-input–multi-output dielectric resonator antenna," *IET Microwaves Antennas Propag.*, 2019 (Accepted).
36. Sharawi, M. S., "Printed multi-band MIMO antenna systems and their performance metrics," *IEEE Antennas Propag. Mag.*, Vol. 55, No. 5, 218–232, 2013.
37. Varshney, G., S. Gotra, V. S. Pandey, and R. S. Yaduvanshi, "Proximity-coupled two-port multi-input-multi-output graphene antenna with pattern diversity for THz applications," *Nano Commun. Netw.*, Vol. 21, 100246, 2019.